**Smart Structures and Systems**, *Vol. 31, No. 6 (2023) 585-599*
https://doi.org/10.12989/sss.2023.31.6.585


# Investigation on vibration behavior of a high-speed railway bridge based on monitoring data

Qingxin Zhu [1,2a], Hao Wang*[1] and Billie F. Spencer Jr. [3]

[1] *Key Laboratory of C&PC Structures of Ministry of Education, Southeast University, Nanjing, 211189, China*
[2] *School of Environment and Architecture, University of Shanghai for Science and Technology, Shanghai, 200093, China*
[3] *Department of Civil and Environmental Engineering, University of Illinois at Urbana-Champaign, Urbana, IL 61801, USA*

(*Received July 30, 2021, Revised March 27, 2022, Accepted June 12, 2023*)

**Abstract.** Field monitoring techniques offer an attractive approach for understanding bridge behavior under in-service loads. However, the investigations on bridge behavior under high-speed train load using field monitoring data are limited. The focus of this study is to explore the structural behavior of an in-service long-span steel truss arch bridge based on field monitoring data. First, the natural frequencies of the structure, as well as the train driving frequencies, are extracted. Then, the train-induced bearing displacement and structural strain are explored to identify the effects of train loads and bearings. Subsequently, a sensitivity analysis is performed for the impact factor of strain responses with respect to the train speed, train weight, and temperature to identify the fundamental issues affecting these responses. Additionally, a similar sensitivity analysis is conducted for the peak acceleration. The results indicate that the friction force in bearings provides residual deformations when two consecutive trains are in opposite directions. In addition, the impact factor and peak acceleration are primarily affected by train speed, particularly near train speeds that result in the resonance of the bridge response. The results can provide additional insight into the behavior of the long-span steel truss bridges under in-service high-speed train loads.

**Keywords:** displacement; field monitoring data; high-speed train; impact factor; long-span steel truss arch bridge; peak acceleration; strain

## 1. Introduction

Railway bridges must operate in harsh environments, experiencing large loads with every train crossing (Quirke *et al*. 2017, Vagnoli *et al*. 2018). Damage often occurs when bridges are subject to these environmental and traffic loads, as well as extreme loads (e.g., earthquake and typhoon), potentially resulting in serious risk to bridge safety and serviceability (Malveiro *et al*. 2018). Thus, maintenance and repair activities are crucial to ensuring operational performance (Xia *et al*. 2013, Leander *et al*. 2010). Accordingly, understanding the bridge behavior under in-service train loads will help operators to focus limited resources on maintaining safe and reliable operation of railway networks.

Structural health monitoring (SHM) techniques have proven effective for conducting condition assessment of as-built bridges in real-time (Wan and Ni 2019, Fujino and Siringoringo 2011). Numerous SHM systems have been installed on large-scale structures (Spencer *et al*. 2004, Ko and Ni 2005). Most of these SHM systems are installed on highway bridges, with only a limited number of practical applications have been found for railway bridges, particularly high-speed railway bridges. Moreover, Moreu and Spencer (2015) indicated that significant differences are found between the behavior of highway bridges and railway bridges, including: (i) the live loads on railway bridges are significantly larger than those on highway bridges, (ii) the impact factor for railway bridges is higher than that for highway bridges, and (iii) interactions of the train-track-bridge system should be considered in the design and maintenance. Thus, information derived from highway bridge SHM systems is of limited use in understanding railway bridge responses.

The dynamic response of railway bridges subjected to high-speed trains is governed by the bridge properties and train parameters (Zhai *et al*. 2019). Many short-term full-scale tests have been conducted to understand the effects of train loads on bridge responses (Leander *et al*. 2010, Su *et al*. 2010). For example, Cantero *et al*. (2016) demonstrated recorded responses of a 36 m long composite bridge to distinguish the effect of various factors on the dynamic response; the study indicated that the combination of axle spacing and train speed is the predominant factor. Note that the impact factor is an important parameter for railway bridge design, assessment, and maintenance, as well as the enforcement of legal train loads (e.g., train weight and train speed) (Gou *et al*. 2022). Tao *et al*. (2018) analyzed the impact factors produced by moving trains based on field test data, and then compared these factors with the suggestions in various codes. Ataei and Miri (2018) carried out 845 dynamic tests on 11 masonry arch bridges in the railway network in Iran to assess the effect of train and

*Corresponding author, Ph.D., Professor,
E-mail: wanghao1980@seu.edu.cn
[a] Ph.D., E-mail: zhuqingxin@usst.edu.cn



ISSN: 1738-1584 (Print), 1738-1991 (Online)

bridge parameters on the impact factor. In addition, bridge deformations (e.g., displacement and structural strain) and vibration (e.g., acceleration) under live loads can benefit the management of bridges and train serviceability (Moreu and LaFave 2012). Numerous studies illustrating the train-induced deformations and vibration, especially the resonant responses, have been conducted (Auersch 2021, Liu *et al*. 2009, Lu *et al*. 2012). For example, Sayed *et al*. (2017) investigated the correlation between bridge acceleration and train speeds to find the train speed that induces resonance of the bridge. While many short-term field tests have been carried out to investigate the behavior of railway bridges under service traffic, particularly focusing the intrinsic effect of train parameters (e.g., train speed and train weight) on the concerned factors of bridges (i.e., impact factor and the peak responses) (Leander *et al*. 2010); however, long-term deployments are still limited due, in part, to high cost. Long-term studies allow environmental variations (e.g., temperature) to be considered (Xu *et al*. 2010). These environmental variations or sudden events can be perceived as randomness in short-term test results.

The object of this work is to investigate the behavior of high-speed railway bridges under in-service train loads using long-term monitoring data, with the goal of understanding issues affecting the dynamic behavior of the high-speed railway bridge. This study addresses steel truss bridges, which are frequently used for longer-span high-speed railway bridges, focusing on the Dashengguan Bridge, located in Nanjing, China. First, dominant frequencies in bridge responses are extracted from the field monitoring data, including the natural frequencies of this bridge and train driving frequencies. Then, train-induced bridge deformations (i.e., bearing displacement and structural strain) are presented to demonstrate the effects of train loads and bearing properties. Subsequently, sensitivity analysis is carried out to investigate the intrinsic effects of train speed, train weight, and temperature on the dynamic response of the bridge (e.g., impact factor and peak acceleration). This study provides useful information regarding the performance of high-speed railway bridges under in-service train loads, which can help prioritize bridge repair and maintenance.

## 2. Long-term monitoring data of the Dashengguan bridge

The Dashengguan Bridge and associated structural health monitoring (SHM) system are introduced individually in this section, forming the foundation of the subsequent investigation.

### *2.1 The Dashengguan Bridge*

The Dashengguan Bridg crosses over the Yangtze River with a total length of 1272 m, as shown in Fig. 1. This symmetrical continuous steel truss arch bridge carries six-lanes of railway traffic in the north bound (NB) and south bound (SB) directions (including the Beijing-Shanghai (B-S) high-speed railway, the Shanghai-Wuhan-Chengdu (S-W-C) quasi-high-speed railway, and the Nanjing Metro Line S3 traffic). Indeed, the Dashengguan Bridge experiences a large amount of traffic during regular operation (approximately 300 high-speed trains per day), forming a critical link in the railroad infrastructures. This heavily transited rail line provides a unique test-bed to achieve the objectives of this research. Three steel arch trusses, supported by reinforced concrete piers, are employed to carry the train loads. Except the middle bridge pier, which has a fixed bearing, spherical steel bearings are installed at the top of the bridge piers. Note that no expansion devices were installed in the bridge. Thus, the accumulative structural responses produced by in-service loads (e.g., traffic and environmental loads) can be significant.

### *2.2 Structural health monitoring (SHM) system*

To gain a deeper understanding of the in-service behavior, as well as ensure the safety, durability, and serviceability of the Dashengguan Bridge, a comprehensive SHM system was permanently installed on this bridge in June 2011. The SHM system can automatically collect train speeds, bearing displacements, structural strains, bridge temperatures, and ambient temperatures. Note that the displacement and temperature are continuously recorded. In contrast, acceleration, strain, and speed are collected only during train crossings. The duration of the measurements depends on the type of train and when sensing was triggered

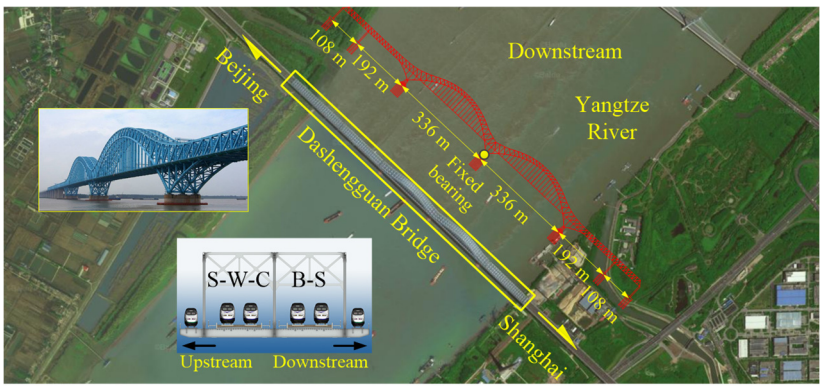


Fig. 1 An aerial view of the Dashengguan Bridge.

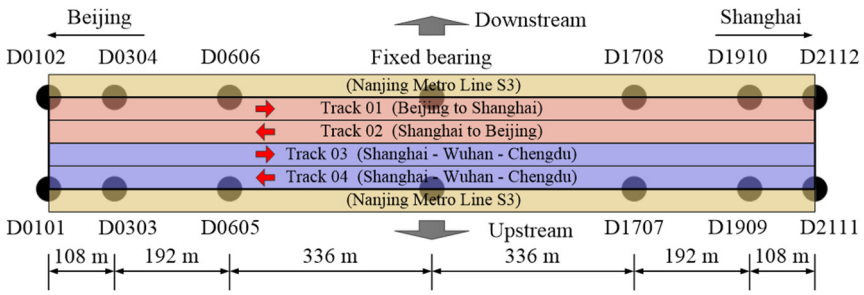


Fig. 2 Layout of displacement sensors mounted on the Dashengguan Bridge

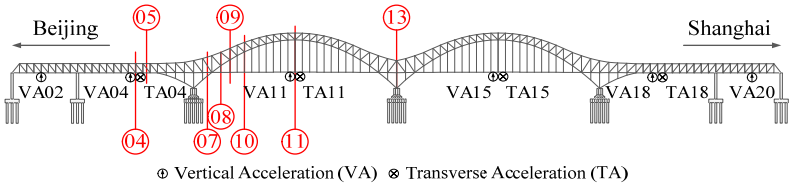


Fig. 3 Acceleration sensor layouts on the Dashengguan Bridge.

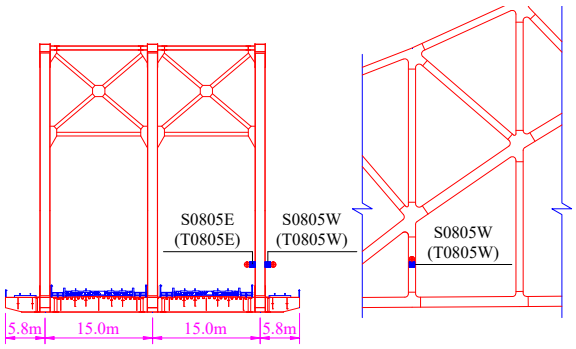


(a) Cross-section 08

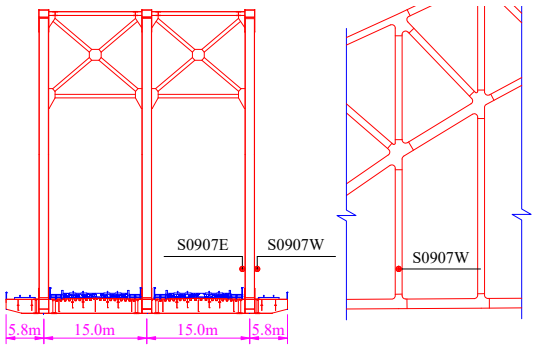


(b) Cross-section 09

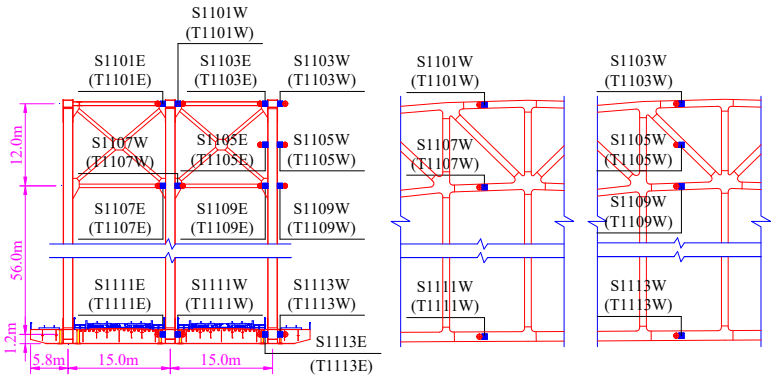


(c) Cross-section 11

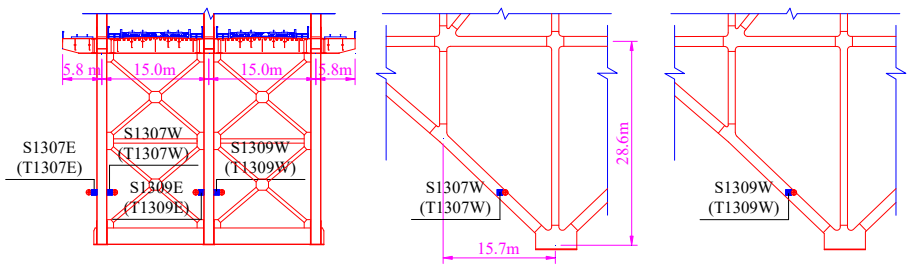


(d) Cross-section 13

Fig. 4 Temperature and strain sensor layouts on the Dashengguan Bridge

to start. The acceleration, strain, displacement, and temperature data are recorded with the sampling frequencies of 200 Hz, 50 Hz, 1 Hz, and 1 Hz, respectively. Fig. 2 shows the layout of displacement sensors. The traffic direction of each lane is also presented in this figure. Fig. 3 depicts the deployment for acceleration sensors, which capture the vertical and transverse accelerations of each span.

In addition, the locations of the cross-sections where the temperature and strain sensors are installed are numerically identified in the figure. The strain and temperature sensors employed in this study are described herein, as shown in Fig. 4. The designations D, S, and T in the labels represent the displacement, strain, and temperature sensors, respectively, followed by the cross-section location number and the identifier for the structural members. Further, E and W represent the east-facing and west-facing plates, respectively. More detailed information regarding the Dashengguan Bridge and its SHM system can be found in Zhu *et al*. (2021).

## 3. Dynamic responses of the Dashengguan Bridge

The recorded acceleration and strain responses are employed to determine natural frequencies and train driving frequencies, which are introduced individually in the subsequent section. Finally, the bridge responses under a typical in-service train loads are presented.

### *3.1 Natural frequencies of the Dashengguan Bridge*

The bridge accelerations under ambient loads are shown in Fig. 5. Transverse accelerations are slightly larger than vertical accelerations, which are mainly produced by crosswind and flowing water. Based on these ambient accelerations, the natural frequencies of the Dashengguan Bridge are extracted using the frequency domain decomposition (FDD) method, as shown in Fig. 6. Herein, the accelerations recorded during the night in January and October are employed to consider the influence of temperature on natural frequencies. In addition, the corresponding average bridge temperatures are 0℃ and 30℃, respectively.

As shown in Fig. 6, the Dashengguan Bridge is more flexible in the vertical direction, with the first vertical mode being around 0.35 Hz. Additionally, the first transverse mode is around 0.51 Hz. Herein, numerous vertical modes are found as the frequency increases. In contrast, most of the transverse frequencies are smaller than 5 Hz. Note that the influence of temperature on structural frequencies is small; the variations of natural frequencies are less than 2% on the interval from 0℃ to 30℃.

### *3.2 Train driving frequencies*

The driving frequencies produced by moving trains are mainly dominated by train parameters (e.g., carriage length) and train speed. Trains cross the Dashengguan Bridge in both directions and with different speeds, ranging from 150 km/h to 200 km/h for the S-W-C line and from 200 km/h to 250 km/h for the B-S line. The typical train contains eight or sixteen carriages, including the locomotive. More detailed information regarding the train parameters can be found in Zhai *et al*. (2015). The driving frequencies produced by moving trains can be obtained as $f = n \cdot l/v$, where $l$ is the carriage length, which is around 25 m; $v$ is the train speed; and $n = 1, 2, 3, \ldots\ldots$ (Ju *et al*. 2009, Wang *et al*. 2019). Herein, the fundamental driving frequency for the Dashengguan Bridge ranges from 1.67 Hz to 3.33 Hz.

The typical train-induced bridge accelerations are shown in Fig. 7. The vertical acceleration is obviously larger than the transverse acceleration. Additionally, the vertical


(a) Main span (b) Side span

Fig. 5 Acceleration responses under ambient excitation


(a) Vertical direction (b) Transverse direction

Fig. 6 Natural frequencies of the Dashengguan Bridge


(a) Sensor V11 (b) Sensor T11

Fig. 7 Train-induced accelerations


(a) Vertical accelerations (b) Transverse accelerations

Fig. 8 The dominant frequencies in train-induced accelerations.

acceleration clearly increases when trains move onto the span where the accelerometers are located. In contrast, the variation in the amplitude of transverse accelerations is small during the crossing process. The dominant frequencies of train-induced accelerations are extracted using the FDD method. The power spectral density (PSD) matrix is obtained by these accelerations (six for vertical direction and four for transverse direction, see Fig. 3) and separated by singular value decomposition (SVD) (Qu *et al.* 2018). If the input is harmonic wave, peak value corresponding to the harmonic wave can be observed in all singular values. The first singular value is always larger than others, which is employed in this study. To ensure the singular values produced by all trains can be observed clearly in one figure, the first singular values are normalized to have a maximum of 1, as shown in Fig. 8; the colorbar displays the normalized value of the first singular value. Note that the Run-Test method indicates the train-induced acceleration is non-stationarity (Wang *et al.* 2016); however, the time-varying characteristics of these frequency components are not concerned herein. The data in Fig. 8 is recorded during several overcast days in February 2013; the temperature variation in these days is negligible, allowing the effect of temperature on structural accelerations and bridge dynamic properties to be ignored. As expected, the loading frequencies identified from the acceleration changes proportionally with the train speed.

Note that resonance occurs when the train loading frequencies coincide with the natural frequencies, which causes the bridge response to increase significantly. For this bridge, the resonance is expected to occur at several train speeds, for example, the resonance corresponding to 1.27 Hz and 2.05 Hz can occur at 31.75 m/s and 51.25 m/s, respectively, as shown in Fig. 8.

### *3.3 Train-induced bridge responses*

To better understand the dynamic properties of the Dashengguan Bridge, the bridge responses under a typical moving train are shown in Fig. 9. The location of selected sensors is also indicated in Fig. 9. This train travels from Shanghai to Beijing on Track 02, with the time where the train enters and exits the Dashengguan Bridge corresponding to approximately 10 s and 38 s, respectively. In addition, the recorded train speed is 68 m/s. As shown in Fig. 9, bridge responses increase significantly when the train crosses this bridge. Note that the acceleration at the sensor VA20 increases suddenly when the locomotive moves on this bridge. In contrast, accelerations at other sensors increase less, being triggered by the vibration of adjacent spans. However, all these accelerations decrease smoothly after the train exits the bridge.

To better understand the measured train-induced accelerations, a time-frequency analysis is conducted using the wavelet transform (WT), and presented in Fig. 10. Herein, the time-frequency spectra for sensors VA02 and VA11 are shown; the spectra for the other sensors are similar to those shown in Fig. 10. For the convenience of the reader, the vertical natural frequencies of this bridge are displayed in Fig. 10(e). The train driving frequencies at 2.72 Hz, 5.44 Hz, 8.16 Hz, and 10.88 Hz are the same for sensors VA02 and VA11, as well as similar to the findings in Fig. 8. The structural responses corresponding to natural frequencies of this bridge are much smaller than the train-induced responses, resulting in the almost imperceptible components at several natural frequencies. These natural frequencies continue to be seen in the spectra after the train leaves the bridge (Spencer *et al.* 2015). In addition, the natural frequencies from Fig. 10(c) are not entirely the same as Fig. 10(d). Generally, global mode means that the complete structure is affected; local mode means that only a small part of the structure oscillates with the corresponding

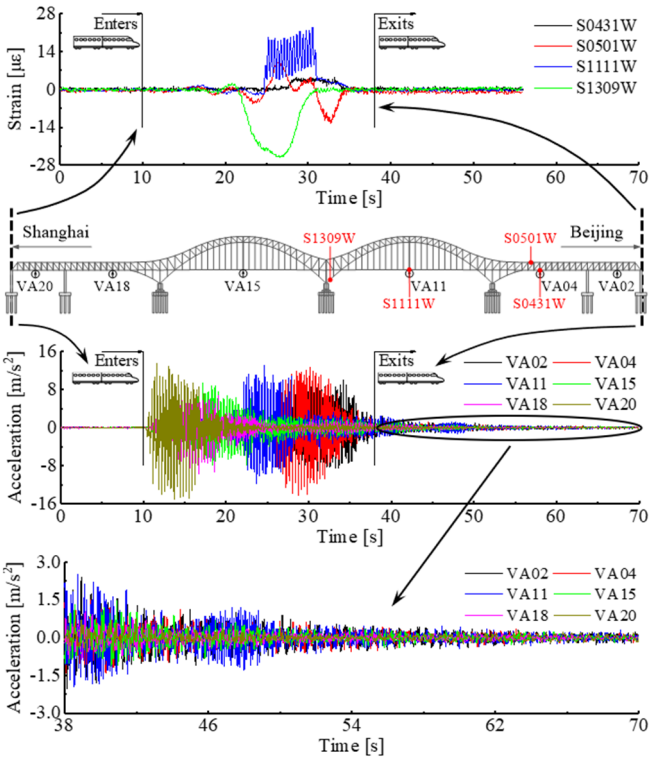


Fig. 9 Bridge responses under a typical moving train (this train enters the bridge at $t$ = 10 s and exits at $t$ = 38 s)

Table 1 The identified damping ratio

| | | | | |
|---|---|---|---|---|
| Global modes | | | | |
| Frequency [Hz] | 2.66 | 5.45 | 8.15 | 11.00 |
| Damping ratio [%] | 1.25 | 2.25 | 1.50 | 1.06 |
| Local modes | | | | |
| Frequency [Hz] | 0.50 | 2.05 | 7.05 | |
| Damping ratio [%] | 2.10 | 0.29 | 0.74 | |

eigenfrequency. Herein, the global means the associated eigenfrequency can be observed in more than half of acceleration sensors, while the local means the corresponding eigenfrequency is only identified in one acceleration sensor. Some global modes (e.g., 2.66 Hz, 5.45 Hz, 8.15 Hz, and 11 Hz) are present in Figs. 10(c) and (d); most of them die out at around 53 s. Several locals (e.g., 0.5 Hz, 2.05 Hz, and 7.05 Hz in Fig. 10(c) and 0.77 Hz, 2.21 Hz, and 4.55 Hz in Fig. 10(d)) are also clearly seen in the vertical direction; these modes are dominant in ambient vibration responses.

After trains exit the bridge, this bridge is subjected to free vibration. In such situations, modal damping ratios can be extracted by applying a bandpass filter to the decaying responses. The decaying responses corresponding to 2.66 Hz, 5.45 Hz, 8.15 Hz, and 11 Hz are obtained using the Butterworth bandpass filter, as shown in Fig. 11(a). However, vibration corresponding to 0.5 Hz, 2.05 Hz, and 7.05 Hz in Fig. 10(c) and 0.77 Hz, 2.21 Hz, and 4.55 Hz in Fig. 10(d) are clearly seen in ambient vibration responses. The random decrement technique (RDT) (He *et al*. 2011) is utilized to obtain the decaying responses in company with the Butterworth bandpass filter, as displayed in Fig. 11(b). Then, the Ibrahim time domain (ITD) technique (Mohanty and Rixen 2004) is utilized to obtain the damping ratio, as summarized in Table 1. Herein, the accelerations induced by 10 trains are employed to calculate the mean damping ratio, and only the local modes observed in Fig. 10 (c) are listed. The locals corresponding to 2.05 Hz and 7.05 Hz have a lower damping ratio. In addition, most of the global modes own a larger damping ratio.

## 4. Train-induced bridge deformations

Bridge deformations (e.g., bearing displacement and structural strain) are principally produced by moving trains (i.e., short-term fluctuations) and temperature variations (i.e., long-term fluctuations), as shown in Fig. 12. Spherical bearings provide longitudinal restraining forces due to the friction, as shown for the simple truss model in Fig. 12. Herein, the left bearing has a lateral restraint, whereas the right bearing does not. The maximum friction force in the right bearing is given by $F_{max}$. The changes in the bearing displacement would be 0 before the bearing friction is overcome by the combination of the train-induced longitudinal force $F_{TR}$ and the temperature-induced force $F_{TE}$. In addition, train-induced longitudinal forces and temperature variations can also affect structural strains. The train-induced longitudinal force mainly affects the structural members, contributing significantly to the longitudinal stiffness of bridges. In contrast, temperature equal influences on the steel members in all directions. Note that vertical train loads are the dominant loads during the train crossing, producing the main component in structural

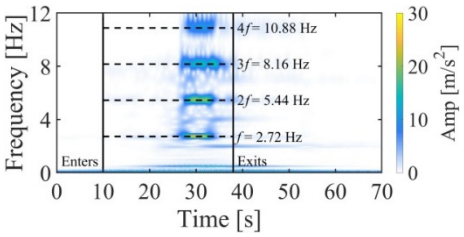


(a) Train-induced acceleration at VA02

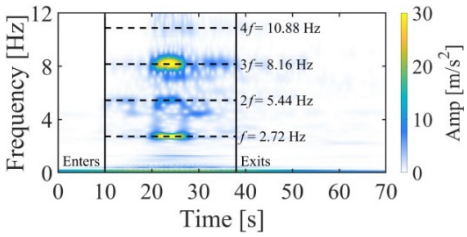


(b) Train-induced acceleration at VA11

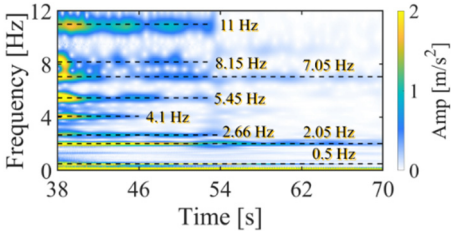


(c) Acceleration at VA02 after this train exits the bridge

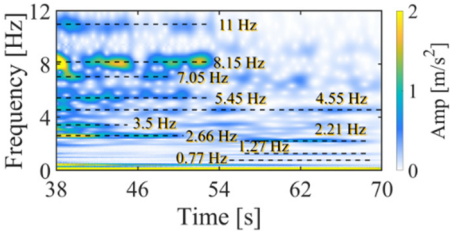


(d) Acceleration at VA11 after this train exits the bridge

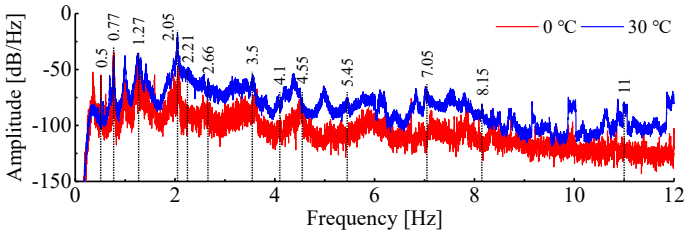


(e) Natural frequencies in the vertical direction

Fig. 10 The time-frequency spectra (this train enters the bridge at $t$ = 10 s and exits at $t$ = 38 s).

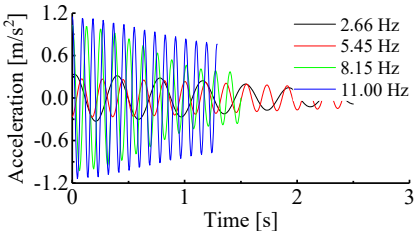


(a) Decaying responses for global modes

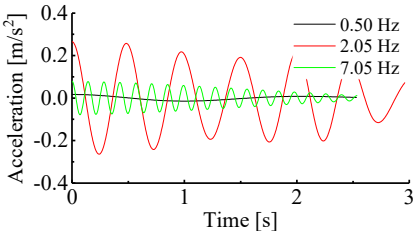


(b) Decaying responses for local modes

Fig. 11 Decaying responses

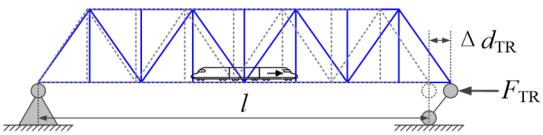


(a) Train-induced deformations

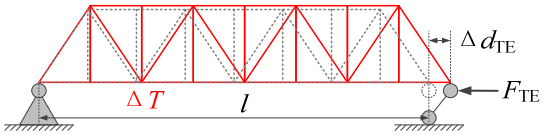


(b) Temperature-induced deformations

Fig. 12 Illustration of bridge deformations

strains. The temperature-induced bridge deformations have been discussed in previous work (Zhu *et al*. 2021); thus, in the remainder of this section, the train-induced bearing displacements and the train-induced structural strains are introduced individually.

### *4.1 Train-induced displacement*

This section describes the effect of moving trains on the bearing displacement. As mentioned previously, the direction of train-induced longitudinal force is dictated by the train direction. Herein, the crossing trains are classified into two general categories: (i) the train moving in the same direction as the previous train (i.e., a north bound (NB) train after another NB train and a south bound (SB) train after another SB train), and (ii) the train moving in the opposite direction of the last train (i.e., a SB train after a NB train and a NB train after a SB train).


(a) Trains moving in the same direction (b) Trains moving in opposite directions

Fig. 13 The train-induced displacement ("N" and "S" in the identifier represent north bound and south bound, respectively)


(a) Trains moving in the same direction (b) Trains moving in opposite directions

Fig. 14 Strain measurements of the bottom chord member S1127 under in-service trains ("N" and "S" in the identifier represent north bound and south bound, respectively)

Fig. 13 shows the autonomous monitoring data at measurement point D0605 for these typical trains crossing the Dashengguan Bridge. The average result for these segments is also shown in Fig. 13 for comparison using solid lines. These datasets are taken from data recorded on October 1st, 2013. Note that the initial values of all data segments are set to zero. The results in each dataset are nearly identical. If the train moves in the same direction as the previous train, the magnitude of the bearing displacements exhibit responses that increase to a peak and then return to the initial level, as shown in Fig. 13(a). The average maximum magnitude for the North-North train is 1.64 mm, whereas for the South-South trains it is 1.42 mm. In contrast, when two consecutive trains are in opposite directions, the bearing plates will move in the opposite direction, too; the average magnitude of residual displacement of the bearing is 2.88 mm, as seen in Fig. 13(b).

Train-induced and temperature-induced bearing displacements potentially result in the abrasion of bearings. The average train-induced bearing motion associated with each train crossing is approximately 3 mm, and roughly 300 trains cross the Dashengguan Bridge each day. On this basis, the daily train-induced motion for bearing D0605 is around 900 mm. Zhu *et al*. (2021) also examined the temperature-induced bearing motion, which is about 4.0 mm/°C for bearing D0605. The average daily temperature variation at the Dashengguan Bridge is around 15 /°C, resulting in a daily temperature-induced motion for this bearing of approximately 120 mm. Therefore, the abrasion of bearings due to in-service trains is more significant than the abrasion associated with temperature variations. Moreover, because the centre bearing is fixed, the bearings away from the centre will experience more abrasion, resulting in higher potential for failure.

### *4.2 Train-induced structural strains*

Train loads produce the main component of the structural strains. Chord members are influenced by the vertical forces, as well as the longitudinal forces, induced by the train. However, the vertical members, which are employed to transfer the load from the bottom chord members to the main steel truss, are only influenced by the vertical train-induced forces. Accordingly, the train-induced strains in chord members and vertical members are investigated separately.

#### *4.2.1 Chord members*

First, the strain responses are examined for the bottom chord member S1127, which is located in the middle of the main span at the Beijing side, as shown in Fig. 3. To focus on the axial strain in the chord member, the strains measured from sensors S1127E and S1127W are averaged together and plotted in Fig. 14. The static strain due to the initial dead loads is not included, because the sensors were mounted after the completion of bridge construction; therefore, the initial value for all data segments is set to zero. Similar to the train-induced displacements, these datasets are also classified into two general categories (i.e., consecutive trains moving in opposite directions and consecutive trains moving in the same direction). The mean strain in this chord, calculated for more than 30 trains, is also shown in Fig. 14 as a solid line. Fig. 14(a) demonstrates that the structural strains nearly return to zero if the two consecutive trains move in the same direction. In contrast, residual strain in is observed in Fig. 13(b) after passing of the second train for the case of two consecutive trains moving in opposite directions; this residual is due primarily to friction in the bearings. This phenomenon is similar to the findings for train-induced displacements

presented in Section 4.1. Additionally, Fig. 14 shows that the maximum strain in the bottom chord member produced by a single train is less than 15 με, indicating that the bottom chord member is always operating in the linear range. Thus, the train-induced strain in the chord members is negligible, when compared with the temperature-induced strain (more than 100 με), as discussed in Zhu *et al*. (2021).

#### *4.2.2 Vertical member*

Next, the second vertical member in the main span at the Beijing side, S0907 (see Fig. 3), is considered to explore its strain responses under in-service trains. The strains measured from sensors S0907E and S0907W are plotted in Fig. 15; the initial value for all data segments is set to zero. Fig. 15 demonstrates that the structural strains nearly return to zero after trains exit the bridge. Thus, the friction force in bridge bearings would not affect the structural strains in the member, which has small contributions to the longitudinal stiffness of the bridge. In addition, the strain from sensor S0907E is nearly a reflection of the strain from sensor S0907W when trains move on the downstream tracks (i.e., Tracks 01 and 02). Therefore, the axial strain in the vertical member, calculated by averaging the strains measured from sensors S0907E and S0907W, is around 0. These trains only produce bending moments in this member. In contrast, the trains moving at the upstream side (i.e., Tracks 03 and 04) produce both axial strains and bending moments in the member S0907. Note that the maximum strain is around 35 με, which is significantly less than the yield strength of steel, as well as smaller than the temperature-induced strains.

## 5. Impact factor for the steel truss bridge

The impact factor is an essential parameter in the design of railway bridges (AREMA 2016). The impact factor is defined as the maximum ratio of the dynamic response to the static response and given by

$$IF = \max\left(\frac{TR_{Dynamic}}{TR_{Static}}\right) \tag{1}$$

where $TR_{\text{static}}$ and $TR_{\text{dynamic}}$ represent the static and dynamic train-induced responses, respectively. The static response $TR_{\text{static}}$ is the pseudo-static train-induced response, whereas the dynamic response $TR_{\text{dynamic}}$ is produced by moving loads applied by the wheels of the train as it crosses the bridge. In the remainder of this section, the impact factor in typical members is examined first. Then, the sensitivity of these impact factors to three parameters (i.e., train speed, train weight, and temperature) is investigated. Note that the impact factor is calculated based on the axial strain in structural members; to this end, strains measured on the


(a) The downstream side (b) The upstream side

Fig. 15 Strain measurements of the vertical member S0907 under in-service trains ("E" and "W" in the identifier represent sensors S0907E and S0907W, respectively)

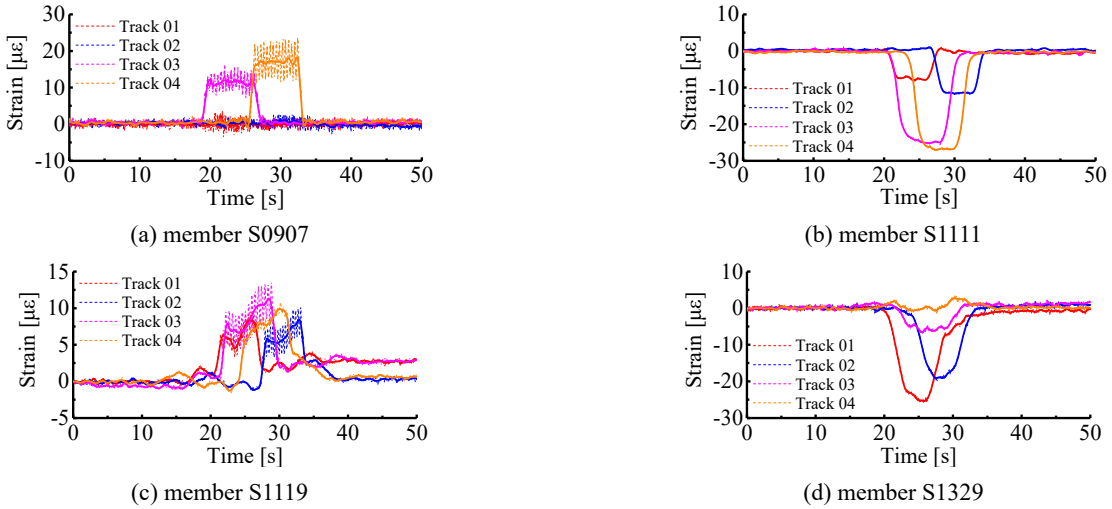


(a) member S0907 (b) member S1111

(c) member S1119 (d) member S1329

Fig. 16 Tran-induced strain responses in typical structural members; the dashed lines correspond to the recorded strain responses, whereas the solid lines represent the pseudo-static response

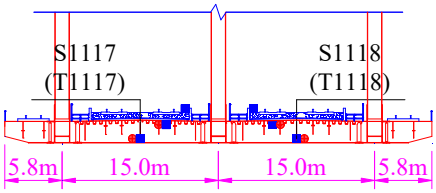


(a) Sensor layouts in the cross-section

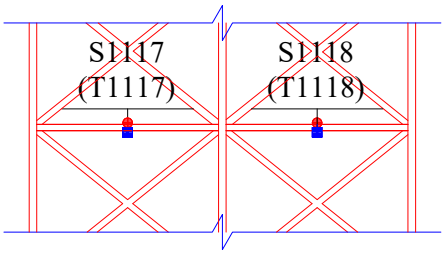


(b) Sensor layouts in the bottom truss

Fig. 17 Sensor layouts for the fully symmetric structural members

same member are averaged together. For example, the axial strain is assumed to be the mean of strains in the east-facing and west-facing plates.

### 5.1 Impact factor for structural members

Fig. 16 depicts the axial strains in typical structural members (including a vertical member S0907, a top chord member S1111, a bottom chord member S1119, and a member adjacent to the middle bearing S1329) under in-service trains moving on different tracks. Again, the axial strain is taken as the mean of strains in the east-facing and west-facing plates. In addition, the pseudo-static response is treated as the time-varying trend of the strain response, which is extracted using a multilevel wavelet decomposition. Accordingly, the measured strain responses and extracted pseudo-static responses are compared using dashed and solid lines. Note that the difference between these two signals represents the dynamic responses.

Fig. 16 illustrates that these structural strains exhibit distinct differences even under the same trains. The bottom chord member S1119, located in the middle truss, experiences similar influences from trains moving on the four tracks. In contrast, the other three members are mainly influenced by the trains moving on the adjacent tracks. For example, S0907 and S1111, located on the upstream truss, are mainly affected by trains on Tracks 03 and 04; S1329 is in the middle truss and sees more effects from trains moving on Tracks 02 and 03. In particularly, trains moving on Tracks 01 and 02 have nearly no influence on the axial strain in member S0907. Similarly, the symmetric member would not see effects from trains moving on Tracks 03 and 04.

The strain range for the vertical members is reasonably large when trains are on Tracks 03 and 04. A similar phenomenon occurs in S1119 when trains move on Tracks 02 and 03. The peaks in these strains correspond to the bogies under the locomotive and carriages. Herein, the difference in the bogie weight between locomotives and carriages is small. The previous valleys and peaks are generated by this train moving on the previous spans. In contrast, the structural strain in the members S1111 and S1329 is quite smooth, indicating that the recorded response features mainly a static contribution with little or no dynamic component. Therefore, the fatigue damage of vertical and bottom members are more sensitive to cyclic wheel loads than the top chord members and members adjacent to the middle bearing.

The impact factors for these members can be estimated intuitively based on Eq. (1). The impact factors for members S1111 and S1329 are almost 0. However, the impact factor for member S0907 reaches 0.3 when trains move on Track 04, and the impact factor for member S1119 is over 0.4 for trains on Tracks 02 and 03. Indeed, impact factors for the Dashengguan bridge are found to range as high as 0.62 for nonresonance and as high as 0.72 for resonance (e.g., in members S1117 and S1118), which will be presented in more detail in the following subsection. The local actions of the wheel loads may account for this phenomenon; impact factors of the member experiencing direct train loads are larger than the indirect member. Thus, this study suggests that the members in truss bridges should be designed with different impact factors. Note that although the impact factors for members the various members are significant, the maximum structural stresses are still much lower than the allowable stress.

### 5.2 Sensitivity of impact factor

This section investigates the sensitivity of impact factors to three factors, which are train speed, train weight, and temperature. Herein, a pair of fully symmetric structural members, which are located in the middle of the main span on the Beijing side (see Fig. 3), S1117 and S1118, is employed, as shown in Fig. 17, and are assumed to share the same dynamic characteristics. The reason for this selection is because the speed range of each track (i.e., ranging from 150 km/h to 200 km/h for the S-W-C line and from 200 km/h to 250 km/h for the B-S line) is too narrow for the sensitivity analysis of impact factors with respect to train speed. The sensitivity results will be presented individually in subsections.

#### 5.2.1 Sensitivity of the impact factor to train speed

Fig. 18 shows the effects of train speed on the impact factor for the selected structural members. The impact factor increases with increasing train speed. In particular, a prominent peak corresponding to 52 m/s is observed. The phenomenon is because resonance occurs when the train driving frequency coincides with the natural frequencies of the bridge. Thus, resonance can significantly increase the impact factor (reaching nearly 40% over adjacent values), which should attract close attention from railway bridge design and maintenance personnel.

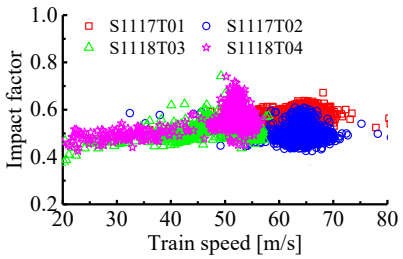


Fig. 18 The relationship between impact factor and train speed ("Txx" represents the track number)

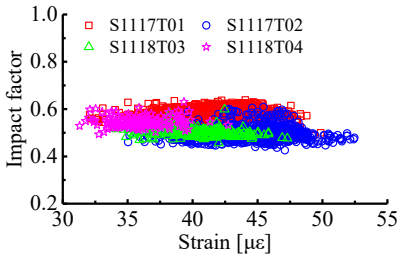


Fig. 19 The relationship between impact factor and average bogie load ("Txx" represents the track number)

### *5.2.2 Sensitivity of the impact factor to train weight*

A sensitivity analysis is now performed to assess how the train weight affects the impact factors. The SHM system installed on the Dashengguan Bridge does not record the weight of crossing trains. Li *et al*. (2018) illustrated vehicle-induced cable tension is determined by vehicle loads and influence lines. Similarly, Wu *et al*. (2018) reported strain responses of the structural strain are influenced by vehicle loads and structural influence lines. Influence lines comprehensively reflect the boundary conditions, geometric properties, and material properties of a structure, which change slightly during the normal operation. In addition, Wang *et al*. (2019) demonstrated that the integral area of strain response represents the gross train weight. However, train-induced dynamic responses significantly influence the integral area (see Fig. 17). Thus, the average pseudo-static strain responses are employed to represent a relative measure of the average weight of bogies. The pseudo-static response is extracted using the multilevel wavelet decomposition. Then, the *k*-means clustering, where *k* equals 2, is operated to divide the pseudo-static response into two parts. The cluster center with the higher magnitude of center is employed as the average pseudo-static strain response, representing the average bogie loads of trains. In addition, to eliminate the influence of train speeds on impact factors, the trains with speeds ranging from 64 m/s to 66 m/s for Tracks 01 and 02, as well as 54 m/s to 56 m/s for Tracks 03 and 04, are utilized by assuming each group shares the similar dynamic characteristics. Accordingly, the relationship between the impact factor and the average pseudo-static strain response (i.e., average bogie loads) is illustrated in Fig. 19. The changes in the impact factor for these trains are relatively small, indicating that the impact factors are almost independent of the bogie loads. Therefore, the train-induced dynamic response changes proportionally with the train weight.

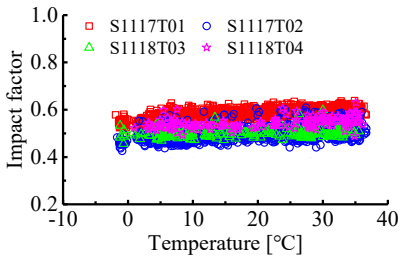


Fig. 20 The relationship between impact factor and average bridge temperature ("Txx" represents the track number)

Table 2 The results from linear regression for the relationship between impact factor and temperature

| Track number | T01 | T02 | T03 | T04 |
|---|---|---|---|---|
| Slope | 0.0013 | 0.0010 | 0.0001 | 0.0007 |
| Squared correlation coefficient | 0.5532 | 0.3780 | 0.0517 | 0.2534 |
| r-squared value | 0.3061 | 0.1429 | 0.0027 | 0.0642 |

### *5.2.3 Sensitivity of the impact factor to temperature*

The relationship between the impact factor and average bridge temperature is shown in Fig. 20 for several representative members. Similar to the previous section, the data employed in Fig. 19 is chosen to eliminate the effect of train speeds on the impact factor. In addition, the results from linear regression of the data are summarized in Table 2. Increases in temperature are seen to result in a modest linear increase in the impact factor. This phenomenon may because the elastic modulus decreases slightly with temperature increase (Xue *et al*. 2020).

## 6. Peak accelerations

This section investigates the sensitivity of peak accelerations of the Dashengguan Bridge to three factors: train speed, train weight, and temperature. Herein, the acceleration sensors mounted on the half-bridge on the Shanghai side are employed. Note that a low-pass filter with the stopband frequency of 45 Hz is applied for the recorded acceleration. In addition, the peak acceleration is denoted as the mean of the first six largest magnitudes to eliminate outliers. These results will be presented individually in the following subsections.

### *6.1 Sensitivity of peak accelerations to train speeds*

Based on the measured train-induced accelerations and train speeds, the variations in peak accelerations with train speeds are shown in Fig. 21. The acceleration in the vertical direction is significantly larger than that in the transverse direction, which is consistent with the results shown in Fig. 7. The highest peak accelerations, in all directions, occurs for sensor VA02. Additionally, the peak acceleration increases for trains running at higher speeds. Trains on

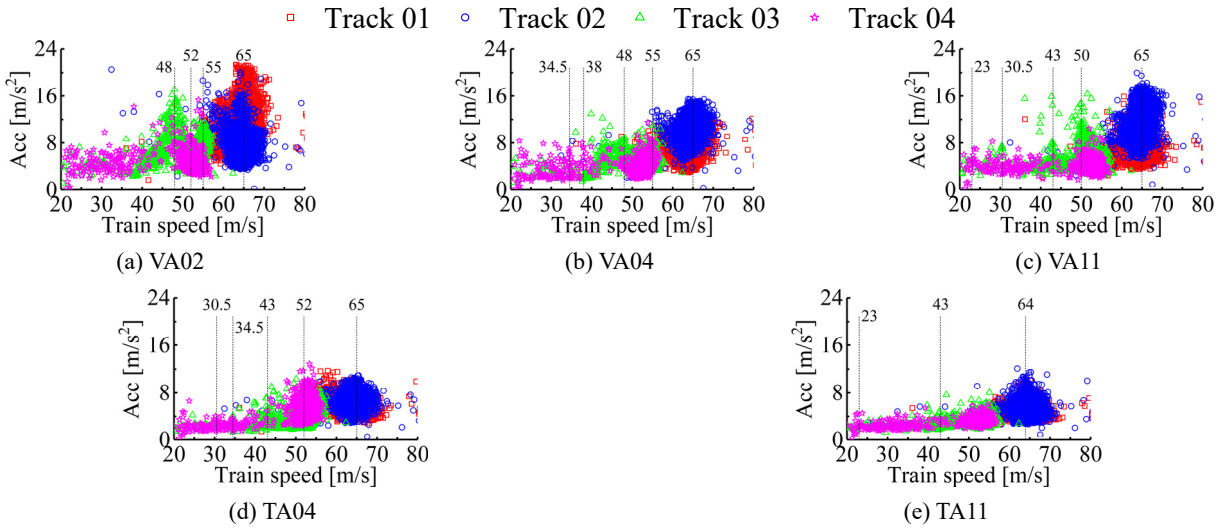


Fig. 22 The relationship between the peak train-induced transverse acceleration and the corresponding peak vertical acceleration (R2 and Corr2 represent the r-squared value and squared correlation coefficient, respectively)

Tracks 01 and 02 typically run at relatively high speeds (mostly over 55.56 m/s), resulting in larger accelerations than for the trains on Tracks 03 and 04. The relationship between the bridge acceleration and train speed provides evidence for the harmonic vibration; the resonance causes the bridge accelerations to increase significantly. As seen in Fig. 21, more peaks corresponding to resonance responses are visible in Fig. 21 than Fig. 18; the peak accelerations at these specific train speeds increase significantly, such as 50 m/s and 65 m/s. Moreover, resonance can also be observed at moderate speeds, and the first critical speed is around 23 m/s. Thus, Fig. 21 can provide reliable reference for estimating the resonances of this truss bridge (both in the vertical and transverse directions) and identifying the critical speeds under in-service trains. Moreover, as seen in Fig. 22, the relationship between the peak train-induced transverse acceleration and the corresponding peak vertical acceleration is modeled using a linear model (see the solid lines in Fig. 22). In addition, the r-squared value ($R^2$) and squared correlation coefficient ($Corr^2$) are also given in the figure. These results indicate that the peak transverse acceleration is relative to the peak vertical acceleration, which is consistent with the findings of Moreu and Spencer (2015).

### 6.2 Sensitivity of peak accelerations to train weights

The changes in the peak acceleration with the variations of train weight are investigated in this subsection. Similar to Section 5.2.2, the average pseudo-static strain response in sensors S1117 and S1118 is used as a surrogate for the average bogie loads for the trains. Accordingly, the relationship between peak acceleration and corresponding average pseudo-static strain is shown in Fig. 23. In addition, the results from linear regression of the data are summarized in Table 3, where the squared correlation coefficient ranges from $2.9 \times 10^{-6}$ to 0.1964. These results

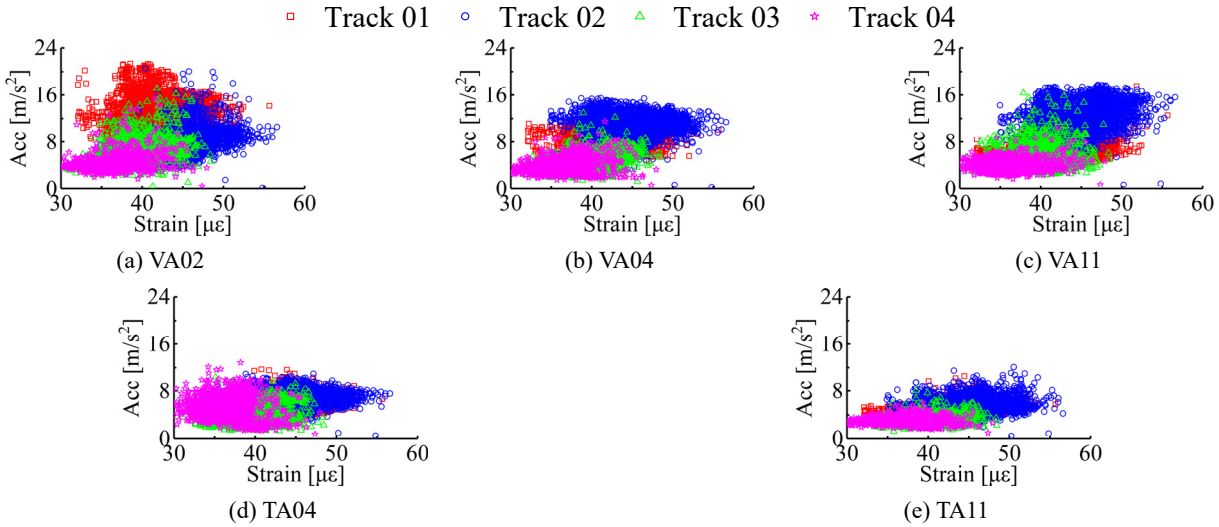


Fig. 23 The relationship between peak acceleration and average bogie load for trains on various tracks

Table 3 The results from linear regression for the relationship between peak acceleration and average bogie load

| Sensor | Parameter | Track | | | |
|---|---|---|---|---|---|
| | | Track 01 | Track 02 | Track 03 | Track 04 |
| VA02 | Squared correlation coefficient | $2.89 \times 10^{-06}$ | 0.1964 | 0.0325 | 0.0605 |
| | Slope | -0.0015 | 0.1599 | 0.1078 | 0.0679 |
| VA04 | Squared correlation coefficient | 0.1179 | 0.0044 | 0.0622 | 0.0375 |
| | Slope | 0.2213 | 0.0205 | 0.0952 | 0.0492 |
| VA11 | Squared correlation coefficient | 0.1456 | 0.0758 | $9.61 \times 10^{-06}$ | 0.0119 |
| | Slope | 0.1859 | 0.1266 | 0.0018 | 0.0219 |
| TA04 | Squared correlation coefficient | 0.1208 | 0.0431 | 0.0393 | 0.0026 |
| | Slope | 0.1366 | 0.0457 | 0.0901 | -0.0193 |
| TA11 | Squared correlation coefficient | 0.1721 | 0.0880 | 0.0327 | 0.0223 |
| | Slope | 0.1111 | 0.0684 | 0.0372 | 0.0187 |

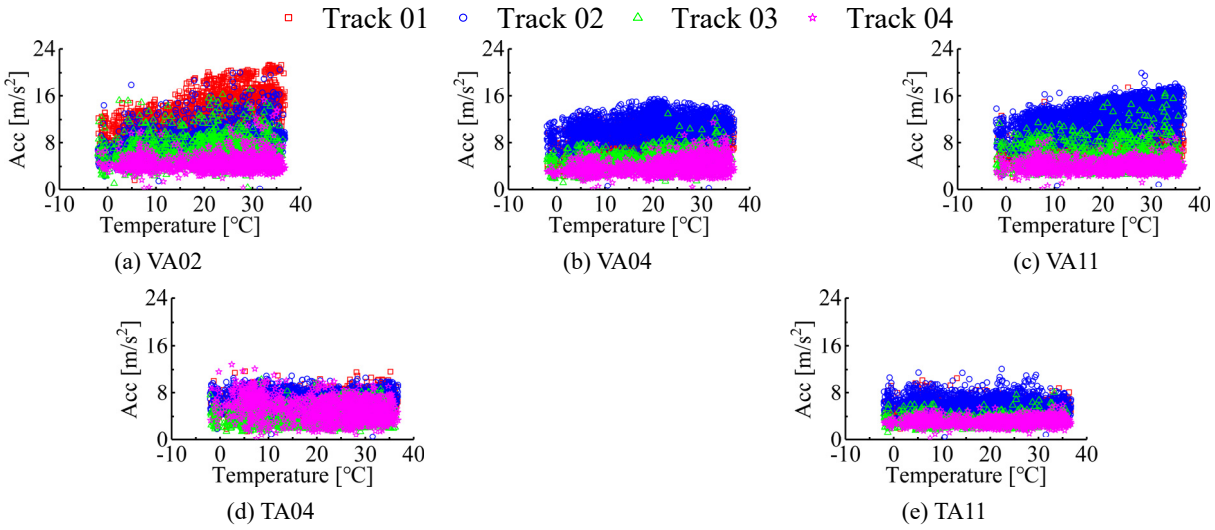


Fig. 24 The relationship between peak acceleration and average bridge temperature for trains on various tracks

Table 4 The results from linear regression for the relationship between peak acceleration and average bridge temperature

| Sensor | Parameter | Track | | | |
|---|---|---|---|---|---|
| | | Track 01 | Track 02 | Track 03 | Track 04 |
| VA02 | Squared correlation coefficient | 0.3750 | 0.1565 | 0.0500 | 0.0060 |
| | Slope | 0.1837 | 0.0826 | 0.0486 | 0.0106 |
| VA04 | Squared correlation coefficient | 0.1151 | 0.0907 | 0.1118 | 0.0918 |
| | Slope | 0.0724 | 0.0539 | 0.0465 | 0.0382 |
| VA11 | Squared correlation coefficient | 0.0897 | 0.2404 | 0.0046 | $4.49 \times 10^{-5}$ |
| | Slope | 0.0483 | 0.1305 | 0.0142 | 0.0007 |
| TA04 | Squared correlation coefficient | 0.0541 | 0.0005 | 0.0260 | 0.0959 |
| | Slope | 0.0303 | -0.0030 | 0.0267 | -0.0580 |
| TA11 | Squared correlation coefficient | 0.3222 | 0.0061 | 0.0073 | 0.0022 |
| | Slope | 0.0159 | -0.0104 | 0.0064 | 0.0029 |

indicate that the peak acceleration is relatively insensitive to increases in train weight.

### 6.3 Sensitivity of peak accelerations to temperature

The relationship between the peak acceleration and average bridge temperature is presented in Fig. 24; the corresponding results for the linear regression are listed in Table 4. Sensor VA02 and VA11 demonstrate a modest correlation between acceleration and temperature, particularly the trains on Tracks 01 and 02, with the squared correlation coefficient ranging from 0.0897 to 0.3750; this influence of temperature is seen to be more pronounced for higher speed trains. However, for the other sensors considered (i.e., VA04, TA04, and TA11) the peak accelerations are relatively insensitive to increases in temperature.

## 7. Conclusions

To offer better understanding of the behavior of the long-span steel truss bridge under in-service high-speed train loads, this study explored the structural behavior of an in-service long-span steel truss arch bridge based on long-term field monitoring data. The train-induced bridge deformations illustrated the friction force in bearings causes residual deformations (e.g., bearing displacement and structural strain in chord members) when two consecutive trains are in opposite directions. Based on the train-induced strain response, the impact factors for different types of members are calculated; the results demonstrated the impact factors for the chord and transverse members in the bottom truss, as well as vertical member, are significant when trains are on adjacent tracks. In addition, the impact factor is mainly affected by train speed, and resonance can significantly increase the impact factor. In addition, the sensitivity analysis was performed for the peak acceleration with respect to the train speed, train weight, and temperature. Similar to the impact factor, the peak acceleration is also mainly affected by train speed, particularly near resonance. Note that bridge temperature has a larger influence on the peak acceleration in the vertical direction than in the transverse direction. These results can validate previous analytical research (e.g., numerical simulations), which can also provide additional insight into the behavior of the long-span steel truss bridges under in-service high-speed train loads.

## Acknowledgments

The authors would like to gratefully acknowledge the supports from the National Natural Science Foundation of China (Grant No. 51978155), the National Ten Thousand Talent Program for Young Top-notch Talents (Grant No. W03070080), the Postgraduate Research and Practice Innovation Program of Jiangsu Province (Grant No. KYCX19_0095), the CSC Scholarship (Grant No. CSC201906090075), and the Fundamental Research Funds for the Central Universities (Grant No. 2242022k30030).

## References

AREMA (American Railway Engineering and Maintenance-of-Way Association) (2016), Manual for railway engineering; American Railway Engineering Association.

Ataei, S. and Miri, A. (2018), "Investigating dynamic amplification factor of railway masonry arch bridges through dynamic load tests", *Constr. Build. Mater.*, **183**, 693-705. https://doi.org/10.1016/j.conbuildmat.2018.06.151

Auersch, L. (2021), "Resonances of railway bridges analysed in frequency domain by the modal-force-excitation, bridge-transfer and axle-sequence spectra", *Eng. Struct.*, **249**, 113282. https://doi.org/10.1016/j.engstruct.2021.113282

Cantero, D., Ülker-Kaustell, M. and Karoumi, R. (2016), "Time–frequency analysis of railway bridge response in forced vibration", *Mech. Syst. Signal Process.*, **76**, 518-530. https://doi.org/10.1016/j.ymssp.2016.01.016

Fujino, Y. and Siringoringo, D.M. (2011), "Bridge monitoring in Japan: the needs and strategies", *Struct. Infrastr. Eng.*, **7**(7-8), 597-611. https://doi.org/10.1080/15732479.2010.498282

Gou, H.Y., Zhao, T.Q., Qin, S.Q., Zheng, X.G., Pipinato, A. and Bao, Y. (2022), "In-situ testing and model updating of a long-span cable-stayed railway bridge with hybrid girders subjected to a running train", *Eng. Struct.*, **253**, 113823. https://doi.org/10.1016/j.engstruct.2021.113823

He, X.H., Hua, X.G., Chen, Z.Q. and Huang, F.L. (2011), "EMD-based random decrement technique for modal parameter identification of an existing railway bridge", *Eng. Struct.*, **33**(4), 1348-1356. https://doi.org/10.1016/j.engstruct.2011.01.012

Ishihara, T., Zhang, D. and Nagumo, Y. (2021), "Numerical study of dynamic response of railway vehicles under tunnel exit winds using multibody dynamic simulations", *J. Wind Eng. Indust. Aerodyn.*, **211**, 104556. https://doi.org/10.1016/j.jweia.2021.104556

Ju, S.H., Lin, H.T. and Huang, J.Y. (2009), "Dominant frequencies of train-induced vibrations", *J. Sound Vib.*, **319**(1-2), 247-259. https://doi.org/10.1016/j.jsv.2008.05.029

Ko, J.M. and Ni, Y.Q. (2005), "Technology developments in structural health monitoring of large-scale bridges", *Eng. Struct.*, **27**(12), 1715-1725. https://doi.org/10.1016/j.engstruct.2005.02.021

Leander, J., Andersson, A. and Karoumi, R. (2010), "Monitoring and enhanced fatigue evaluation of a steel railway bridge", *Eng. Struct.*, **32**(3), 854-863. https://doi.org/10.1016/j.engstruct.2009.12.011

Li, S.L, Wei, S.Y., Bao, Y.Q. and Li, H. (2018), "Condition assessment of cables by pattern recognition of vehicle-induced cable tension ratio", *Eng. Struct.*, **155**, 1-15. https://doi.org/10.1016/j.engstruct.2017.09.063

Liu, K., De Roeck, G. and Lombaert, G. (2009), "The effect of dynamic train–bridge interaction on the bridge response during a train passage", *J. Sound Vib.*, **325**(1-2), 240-251. https://doi.org/10.1016/j.jsv.2009.03.021

Lu, Y., Mao, L., Woodward, P. (2012), "Frequency characteristics of railway bridge response to moving trains with consideration of train mass", *Eng. Struct.*, **42**, 9-22. https://doi.org/10.1016/j.engstruct.2012.04.007

Malveiro, J., Sousa, C., Ribeiro, D. and Calçada, R. (2018), "Impact of track irregularities and damping on the fatigue damage of a railway bridge deck slab", *Struct. Infrastr. Eng.*, **14**(9), 1257-1268. https://doi.org/10.1080/15732479.2017.1418010

Mohanty, P. and Rixen, D.J. (2004), "A modified Ibrahim time domain algorithm for operational modal analysis including

harmonic excitation", *J. Sound Vib.*, **275**(1-2), 375-390. https://doi.org/10.1016/j.jsv.2003.06.030

Moreu, F. and LaFave, J.M. (2012), "Current research topics: Railroad bridges and structural engineering", Newmark Structural Engineering Laboratory Report Series 032. http://hdl.handle.net/2142/34749

Moreu, F. and Spencer Jr, B.F. (2015), "Framework for consequence-based management and safety of railroad bridge infrastructure using wireless smart sensors (WSS)", Newmark Structural Engineering Laboratory, University of Illinois at Urbana-Champaign, Champaign, IL, USA. http://hdl.handle.net/2142/78094

Qu, C.X., Yi, T.H., Li, H.N. and Chen, B. (2018), "Closely spaced modes identification through modified frequency domain decomposition", *Measurement*, **128**, 388-392. https://doi.org/10.1016/j.measurement.2018.07.006

Quirke, P., Bowe, C., OBrien, E.J., Cantero, D., Antolin, P. and Goicolea, J.M. (2017), "Railway bridge damage detection using vehicle-based inertial measurements and apparent profile", *Eng. Struct.*, **153**, 421-442. https://doi.org/10.1016/j.engstruct.2017.10.023

Sayed, M.A., Kaloop, M.R., Kim, E. and Kim, D. (2017), "Assessment of acceleration responses of a railway bridge using wavelet analysis", *KSCE J. Civil Eng.*, **21**(5), 1844-1853. https://doi.org/10.1007/s12205-016-1762-0

Spencer Jr, B.F., Ruiz-Sandoval, M.E. and Kurata, N. (2004), "Smart sensing technology: opportunities and challenges", *Struct. Control Health Monitor.*, **11**(4), 349-368. https://doi.org/10.1002/stc.48

Spencer Jr, B.F., Moreu, F. and Kim, R.E. (2015), "Campaign monitoring of railroad bridges in high-speed rail shared corridors using wireless smart sensors", Newmark Structural Engineering Laboratory, University of Illinois at Urbana-Champaign, Champaign, IL, USA. http://hdl.handle.net/2142/78095

Su, D., Fujino, Y., Nagayama, T., Hernandez Jr, J.Y. and Seki, M. (2010), "Vibration of reinforced concrete viaducts under high-speed train passage: measurement and prediction including train–viaduct interaction", *Struct. Infrastr. Eng.*, **6**(5), 621-633. https://doi.org/10.1080/15732470903068888

Sun, S.W., Sun, L.M. and Chen, L. (2016), "Damage detection based on structural responses induced by traffic load: methodology and application", *Int. J. Struct. Stabil. Dyn.*, **16**(4), 1640026. https://doi.org/10.1142/S0219455416400265

Tao, T.Y., Wang, H., Hu, S.T. and Zhao, X.X. (2018), "Dynamic performance of typical steel truss–railway bridges under the action of moving trains", *J. Perform. Constr. Facil.*, **32**(4), 04018053. https://doi.org/10.1061/(ASCE)CF.1943-5509.0001200

Vagnoli, M., Remenyte-Prescott, R. and Andrews, J. (2018), "Railway bridge structural health monitoring and fault detection: State-of-the-art methods and future challenges", *Struct. Health Monitor.*, **17**(4), 971-1007. https://doi.org/10.1177%2F1475921717721137

Wan, H.P. and Ni, Y.Q. (2019), "Bayesian multi-task learning methodology for reconstruction of structural health monitoring data", *Struct. Health Monitor.*, **18**(4), 1282-1309. https://doi.org/10.1177%2F1475921718794953

Wang, H., Wu, T., Tao, T.Y., Li, A.Q. and Kareem, A. (2016), "Measurements and analysis of non-stationary wind characteristics at Sutong Bridge in Typhoon Damrey", *J. Wind Eng. Indust. Aerodyn.*, **151**, 100-106. https://doi.org/10.1016/j.jweia.2016.02.001

Wang, H., Zhu, Q.X., Li, J., Mao, J.X., Hu, S.T. and Zhao, X.X. (2019), "Identification of moving train loads on railway bridge based on strain monitoring", *Smart Struct. Syst., Int. J.*, **23**(3), 263-278. https://doi.org/10.12989/sss.2019.23.3.263

Wu, B.T., Wu, G., Yang, C.Q. and He, Y. (2018), "Damage identification method for continuous girder bridges based on spatially-distributed long-gauge strain sensing under moving loads", *Mech. Syst. Signal Process.*, **104**, 415-435. https://doi.org/10.1016/j.ymssp.2017.10.040

Xia, Y., Chen, B., Zhou, X.Q. and Xu, Y.L. (2013), "Field monitoring and numerical analysis of Tsing Ma Suspension Bridge temperature behavior", *Struct. Control Health Monitor.*, **20**(4), 560-575. https://doi.org/10.1002/stc.515

Xu, Y.L., Chen, B., Ng, C.L., Wong, K.Y. and Chan, W.Y. (2010), "Monitoring temperature effect on a long suspension bridge", *Struct. Control Health Monitor.*, **17**(6), 632-653. https://doi.org/10.1002/stc.340

Xue, H., Liu, D., Ge, R., Pan, L.B, and Peng, W.J. (2020), "The delay loop phenomenon in high temperature elasticity modulus test by in-situ ultrasonic measurements", *Measurement*, **160**, 107833. https://doi.org/10.1016/j.measurement.2020.107833

Zhai W.M., Liu P.F., Lin J.H. and Wang K.Y. (2015), "Experimental investigation on vibration behaviour of a CRH train at speed of 350 km/h", *Int. J. Rail Transport.*, **3**(1), 1-16. https://doi.org/10.1080/23248378.2014.992819

Zhai, W.M., Han, Z.L., Chen, Z.W., Ling, L. and Zhu, S.Y. (2019), "Train–track–bridge dynamic interaction: a state-of-the-art review", *Vehicle Syst. Dyn.*, **57**(7), 984-1027. https://doi.org/10.1080/00423114.2019.1605085

Zhu, Q.X., Wang, H., Xu, Z.D., Spencer Jr, B.F., Mao, J.X. and Gong, Z.H. (2021), "Investigation on temperature contours for a long-span steel truss arch bridge based on field monitoring data", *J. Civil Struct. Health Monitor.*, 1-19. https://doi.org/10.1007/s13349-021-00479-8

*HJ*